Desalination and Water Treatment
www.deswater.com

doi: 10.5004/dwt.2020.26443

208 (2020) 216–226
December

Magnetically modified activated carbon prepared from pine cones for treatment of wastewater containing heavy metals

Milad Mehrvar[a], Hossein Esmaeili[b,*], Soolmaz Khalili[b]

[a]*Department of Chemical Engineering, Dashtestan Branch, Islamic Azad University, Dashtestan, Iran, email: milad.mehrvar@gmail.com (M. Mehrvar)*
[b]*Department of Chemical Engineering, Bushehr Branch, Islamic Azad University, Bushehr, Iran, Tel. +98 9179885692; emails: esmaeili.hossein@gmail.com/esmaeili.hossein@iaubushehr.ac.ir (H. Esmaeili), soolmazkhalili1991@gmail.com (S. Khalili)*

Received 22 March 2020; Accepted 9 August 2020

ABSTRACT

In this study, activated carbon was prepared from pine cones and then was modified using Fe_3O_4 nanoparticles. Afterwards, the characterization of the nano-adsorbent surface was completely investigated using different analyses such as scanning electron microscopy (SEM), X-ray diffraction, dynamic light scattering, Brunauer–Emmett–Teller (BET), transmission electron microscopy (TEM), and Fourier-transform infrared (FTIR) analyses. BET analysis showed that the specific surface area and the average pore diameter of the adsorbent were 665.27 m^2/g and 2.52 nm, respectively, which shows the aforementioned adsorbent has a mesoporous structure. Also, SEM and TEM analyses showed that the adsorbent size is smaller than 100 nm. The nano-adsorbent was then used as a novel and efficient adsorbent to remove nickel (Ni(II)) and cobalt (Co(II)) ions from aqueous media. The maximum sorption capacities for Ni(II) and Co(II) were also obtained 169.5 and 196.1 mg/g, respectively, which showed significant adsorption capacities for both heavy metal ions. Moreover, the reusability of the adsorbent showed that the AC/Fe_3O_4 nano-composite can be used after five cycles of reuse without a significant reduction in the removal efficiency. Furthermore, the Freundlich isotherm model could better be fitted with the experimental data compared to the Langmuir model. Besides, the thermodynamic study demonstrated that the sorption process was irreversible, physical, exothermic, and spontaneous.

Keywords: Magnetic activated carbon nanocomposite; Heavy metals; Adsorption; Pine cone

1. Introduction

Heavy metals are contaminants produced by human activities in natural processes. The presence of heavy metals in the environment is extremely harmful to human life and cause many problems. Toxic heavy metals can diffuse into the water and food chains and enter the human body through drinking water, eating, and inhaling particles suspended in the air [1]. Some heavy metals are toxic even at very low concentrations [2].

Nickel (Ni) ion is one of the main heavy metals, which causes eczema and allergic reactions [3,4]. Excessive Ni(II) concentration may lead to pulmonary, renal, digestive, and skin problems [5]. Industrial processes such as electroplating, battery production, and mining are the main sources of water contamination by nickel [6]. According to the United States Environmental Protection Agency (USEPA), the permissible value of nickel ion in treated wastewater and drinking water are 4.1 and 0.1 mg/L, respectively.

* Corresponding author.

Also, cobalt (Co) ion is necessary for the human body, but an excessive amount of cobalt ion can cause many problems for human health, including low blood pressure, lung problems, paralysis, diarrhea, and bone defects [7,8]. Cobalt and its salts have many applications in nuclear medicine, electroplating industries, in the production of semiconductors, ceramic glazes, and colored utensils and glasses [9,10]. According to the toxicity, adverse impacts, and stability of heavy metals, their removal from wastewater is necessary to protect the environment [7,8,11].

In recent years, various methods have been used to remove heavy metals from wastewater including electrochemical, chemical precipitation, ion exchange, membrane filtration, coagulation–flocculation, floating, and adsorption process [1]. Among these methods, adsorption process is a physico-chemical treatment method and has several advantages such as being cheaper, easy operating conditions, simplicity, and flexibility in design, and is not sensitive to contaminants and toxic compounds. Also, other major benefits of this method are included the effluent production with high-quality and the absence of hazardous materials like ozone and free radicals [11]. Activated carbon (AC) is the most important adsorbent for recovery and removal of metal ions from aqueous solutions because it is an excellent adsorbent and also has a high adsorption capacity, pore structure, and high specific surface area [12–14]. Recently, a great deal of attention has been made to improve the surface properties of AC. To do this, magnetic nanoparticles (e.g., magnetite (Fe_3O_4), maghemite (γ-Fe_2O_3), and hematite (α-Fe_2O_3)) are applied to facilitate the separation of both adsorbent and adsorbate from aqueous solution [15]. Also, magnetic nanoparticles have a high specific surface area due to their small particle sizes [16–18]. Moreover, magnetic nanoparticles can be easily recovered and reused in the adsorption of pollutants [19].

There are several adsorbents in the literature for the removal of heavy metals from aqueous solutions including silica/activated carbon composite [12], γ-Fe_2O_3@chitosan [15], bentonite/Fe_3O_4 nanocomposite [16], CaO/Fe_3O_4/SDS nanocomposite [18], clay@$MnFe_2O_4$ composite [20], polyhydroxylbutyrate/carbon nanotubes [21], chitosan/Fe_3O_4 nanocomposite [22], etc.

The main purpose of the present research was to investigate the removal of nickel and cobalt ions from aqueous solution using the AC/Fe_3O_4 nano-adsorbent. To do this, the effect of pH, temperature, and type of buffer on the adsorption of nickel and cobalt from aqueous solution was investigated. Also, thermodynamic and equilibrium studies of the adsorption process were done. To the best knowledge of the authors, it is the first study on the removal of Ni(II) and Co(II) ions from aqueous solution using the AC/Fe_3O_4 nano-adsorbent.

2. Materials and methods

2.1. Chemicals

The characteristics of the chemicals used in the present research and their manufacturers are presented in Table 1.

2.2. Stock solutions

To prepare nickel and cobalt stock solutions at a concentration of 1,000 mg/L, 0.496 g of $Ni(NO_3)_2{\cdot}6H_2O$, and 0.493 g of $Co(NO_3)_2{\cdot}6H_2O$ were separately poured in 250 mL volumetric flasks and distilled water was added to raise the volume to 100 mL. To prepare solutions with lower concentrations of Ni(II) and Co(II), double distilled water was used. NaOH and HCl (0.1 M) and a pH meter (Metrohm 632) were also used to adjust the pH values of the solutions.

2.3. Preparation of activated carbon

Pine cones were used to prepare activated carbon. After collecting the pine cones, they were transferred to the laboratory and crushed. The pine cones were then thoroughly washed to remove excess material and dust and placed in an oven at 105°C for 1 h. The following steps were performed to convert pine cones to activated carbon. Afterwards, 50 g of the dried pine cone chips were mixed with phosphoric acid (95%) with a mass ratio of 1:10 so that the surfaces of the pine cone chips were thoroughly impregnated with the acid. The solution was transferred to a furnace and its temperature was gradually raised to 900°C for 3 h. The furnace was then turned off for an hour so that the temperature slowly declined to the ambient temperature. The produced carbon was washed until its pH increased above 6.5. The final product was put in the oven at 120°C for 1 h, crushed using a laboratory mortar and pestle, passed through 20, 30, 40, and 50 mesh sieves, and stored in a glass bottle to prevent moisture absorption. Then, 20 mL of nitric acid (65%) was used to saturate 0.5 g of the activated carbon powder. To homogenize the solution, it was placed in an ultrasonic bath at 80°C for 3 h.

Table 1
Materials utilized in preparing the nano-adsorbent and nickel and cobalt solutions

Material	Chemical formula	Manufacturer	Purity
Phosphoric acid	H_3PO_4	Merck of Germany	>96%
Nitric acid	HNO_3	Merck of Germany	>65%
Iron(III) nitrate	$Fe(NO_3)_3$	Merck of Germany	>99%
Nickel(II) nitrate	$Ni(NO_3)_2{\cdot}6H_2O$	Merck of Germany	>99%
Cobalt(II) nitrate	$Co(NO_3)_2{\cdot}6H_2O$	Merck of Germany	>99%
Sodium hydroxide	NaOH	Merck of Germany	>99%
Hydrochloric acid	HCL	Merck of Germany	>37%

2.4. Magnetic activated carbon

0.5 g of the AC was filtered and the obtained powder was added to 200 mL of the iron nitrate ($Fe(NO_3)_3$) solution, and the solution was homogenized again in an ultrasonic bath and then filtered using filter paper. The mixture was then put inside an electric furnace at 300°C for 2 h to be purified. Finally, the synthesized adsorbent was separated by an external magnetic field and washed several times with distilled water. Then, the adsorbent was dried in the oven at 105°C and stored in a desiccator to be used later.

2.5. Characterization of the adsorbent

The Brunauer, Emmett, and Teller method (BET, ASPA Model 2020) was used to measure the structural properties of the adsorbent such as specific surface area and pores volume. Also, the X-ray diffractometer analysis (XRD, Bruker AXS D8, Germany) was used to study the crystalline structure of the adsorbent, and Fourier transform infrared spectroscopy (Perkin Elmer spectrum two, FT-IR, USA) was applied to specify the functional groups in the structure of the activated carbon and magnetic activated carbon. Moreover, scanning electron microscopy (SEM, model VEGA II, Brno, Czech Republic) was used to determine the adsorbent morphology before and after adsorption process. Furthermore, dynamic light scattering (DLS, Vasco/Cordouan Technologies, France) was used to obtain particle size distribution of the adsorbent. Besides, transmission electron microscopy (TEM, Zeiss LEO 906, Germany) was utilized to measure particle size of the nanocomposite and determination of the nanocomposite morphology.

2.6. Uptake experiments

The impact of various parameters such as pH (2–10), initial concentrations of nickel and cobalt ions (1–100 mg/L), adsorbent dosage (0.1–5 g/L), and temperature (25°C–55°C) was studied on the sorption of metal ions from aqueous media. Three replications of each experiment were performed and their average was reported.

At the end of the experiments, the AC/Fe_3O_4 particles were separated from the solutions using an external magnetic field (1 tesla), and the amounts of adsorbed metal ions was measured using a flame atomic absorption spectrophotometer (AAS, GBC Avanta model, Australia). Eq. (1) was used to calculate the amounts of adsorbed nickel and cobalt ions [23,24]:

$$R = \left(\frac{C_i - C_0}{C_i} \right) \times 100 \quad (1)$$

where C_i and C_0 are the initial and remaining concentrations of the metal ions, respectively.

3. Results and discussions

3.1. Characteristics and surface features of the nanocomposite

Fig. 1 shows SEM images before and after adsorption process. As shown in Fig. 1a, AC/Fe_3O_4 nano-adsorbent is very rough and has many pores that increase its specific surface area. Also, Fig. 1b demonstrates the surface of the adsorbent after the adsorption process of nickel and cobalt ions. As can be seen, the pores and holes on the adsorbent surface are covered by Ni(II) and Co(II) ions. Moreover, this analysis demonstrates that the particle size of the composite is less than 100 nm.

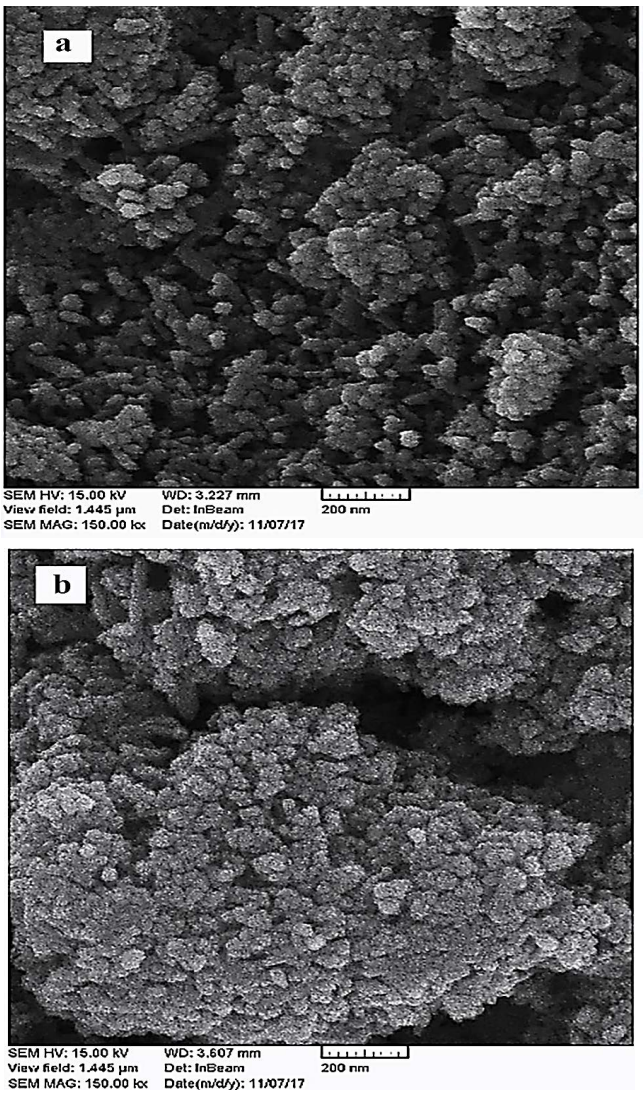

Fig. 1. SEM images of AC/Fe_3O_4 nanocomposite before (a) and after (b) adsorption.

The TEM analysis for AC/Fe_3O_4 nano-adsorbent is also shown in Fig. 2. As shown in this figure, nanocomposite particles are spherical and their size is very fine (less than 50 nm), which shows that the aforementioned composite is on a nanoscale.

Results of BET analysis indicated that the specific surface area, the average pore diameter (APD) and the total pore volume (TPV) of the magnetic activated carbon nanocomposite were 665.27 m^2/g, 2.5232 nm, and 0.4197 cm^3/g, respectively. The results of BET analysis are presented in Table 2. Fig. 3 presents Barrett, Joyner, and Halenda (BJH) and BET analysis of the adsorbent. According to the results,

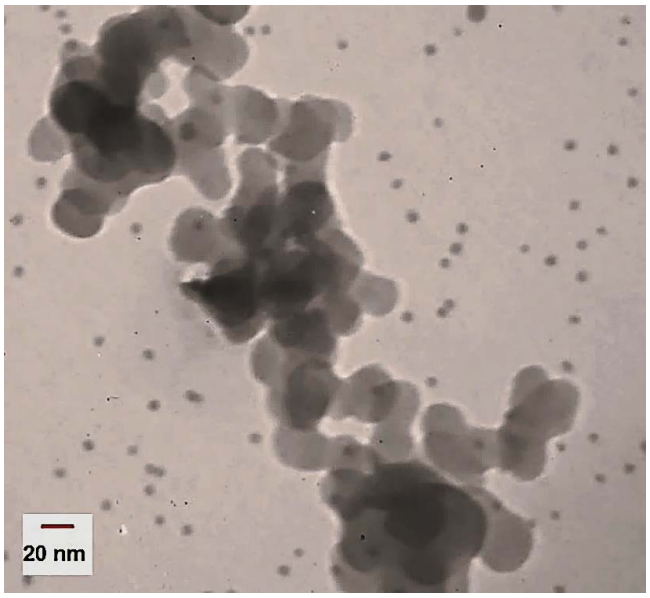

Fig. 2. TEM analysis of AC/Fe_3O_4 nanocomposite.

Table 2
BET results for the magnetic activated carbon nano-adsorbent

Specific surface area (m^2/g)	665.27
Mean pore diameter (nm)	2.5232
Total pore volume (cm^3/g)	0.4197

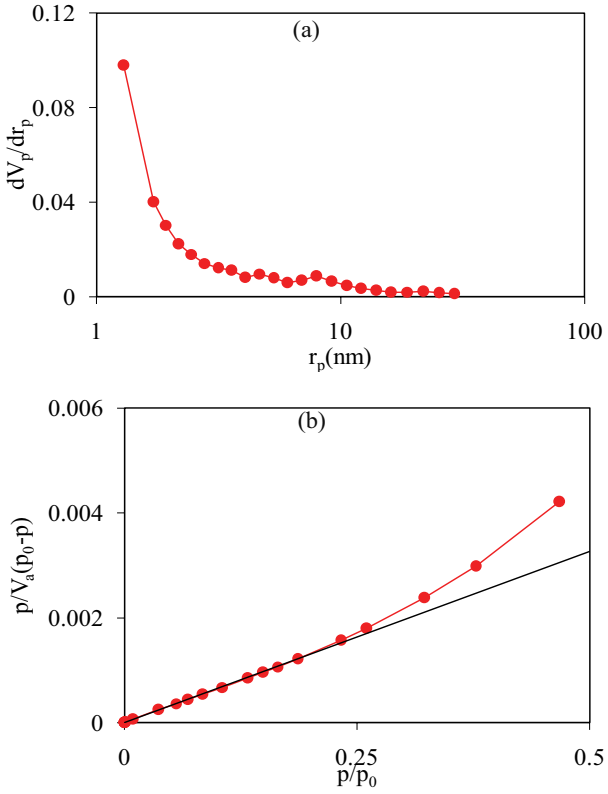

Fig. 3. BJH (a) and N_2 adsorption/desorption isotherm and (b) plots for the magnetic activated carbon nanocomposite.

the adsorbent had a very high specific surface area. Also, the adsorbent is a mesoporous material because its APD is between 2 and 50 nm. Based on the BET analysis, it can be said that this adsorbent can be used to treat wastewater containing Ni(II) and Co(II) ions. According to Fig. 3b, the type of N_2 adsorption/desorption isotherm included two parts. At low relative pressure (P/P_0), the increase in the adsorption rate was slow, showing monolayer sorption. However, at high relative pressure, the increase in the adsorption rate became faster due to the capillary condensation [25]. Also, by comparing the specific surface area of the aforementioned nano-composite (665.27 m^2/g) with previous studies such as bentonite/Fe_3O_4 nanocomposite (52.18 m^2/g) [16], bentonite clay@$MnFe_2O_4$ composite (95.92 m^2/g) [19], eggshell nano-particle (5.6 m^2/g) [23], magnetic nanoparticles@SiO_2 (25.21 m^2/g), magnetic nanoparticles@SiO_2@3-glycidoxypropyltrimethoxysilane-branched polyethyleneimine (38.33 m^2/g) [26] and $NiFe_2O_4$/hazelnut-shell/AC (288 m^2/g) [27], can be concluded that the nanocomposite used in this study has a significant specific surface area compared to other composites.

Fig. 4 also shows the FTIR spectrum of the adsorbent. As shown in this Fig. 4, no tangible changes occurred in the adsorbent before and after the adsorption process. According to the Fig. 4, two peaks were observed at 3,495 cm^{-1} and in the range of 1,500–1,700 cm^{-1}, which are attributed to the stretching vibrations of the O–H bond. Also, a peak at 2,900 cm^{-1} was seen, which is attributed to the vibrations of the C–H bond [19]. Moreover, a peak in the range of 500 cm^{-1} was observed attributing to the Fe–O bond stretching vibration and also a peak at 1,000 cm^{-1} was seen, which is related to the O–C–O functional group [18]. Generally, this analysis suggests that the adsorption process can be done physically.

Fig. 5 presents the XRD pattern of the magnetic activated carbon nano-adsorbent. The peaks at 2θ of 26.45°, 35.8°, 43.3°, 54.25°, 57.4°, and 63.6° are related to the 220, 311, 400, 422, 511, and 440 crystalline phases. Since the reaction is single-phase and the activated carbon is not read in the XRD spectrum, all peaks are related to the Fe_3O_4 spectra, which match with standard card number 0449–075–01 [16]. This analysis indicated that the aforementioned nanocomposite has a crystalline structure.

There are three methods for performing a DLS analysis including Pade-Laplace, Cumulants, and sparse Bayesian learning (SBL). The SBL method was used in this research. DLS analysis of the adsorbent is presented in Fig. 6. This analysis indicates that the average scattering intensity of the adsorbent nano-particles, the mean number of adsorbent nano-particles, and the average volume of the adsorbent nano-particles were 50.72 nm, 16.01 nm, and 23.29 nm, respectively. Based on the obtained results, the adsorbent particles are on a nano-scale.

3.2. Impact of pH

The functional groups on the adsorbent surface gain a positive or negative charge by changing the pH values.

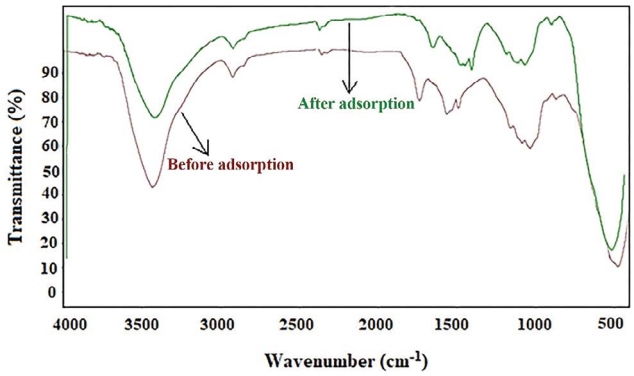

Fig. 4. FTIR analysis AC/Fe_3O_4 before and after adsorption.

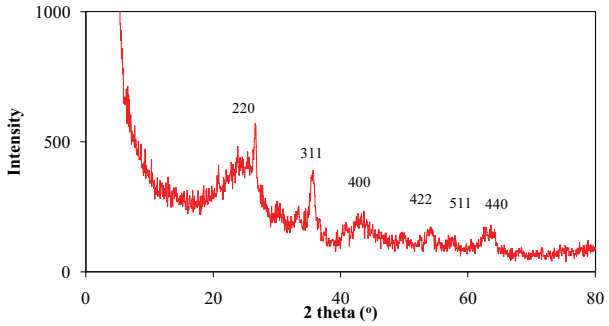

Fig. 5. XRD image of the magnetic activated carbon nano-adsorbent.

At low pH values, there will be a repulsive force between hydrogen (H^+) and metal ions in the solution because both have positive charges. This will increase the competition between them. However, the presence of a large number of hydrogen ions compared to metal ions leads to their greater inclination to occupy the active sites on the nano-adsorbent surface. As a result, the removal percentage of metal ions is low [28]. In the present study, the impact of pH (2, 3, 4, 5, 6, 7, 8, 9, and 10) was studied on the adsorption of nickel and cobalt ions from aqueous solutions using the magnetic activated carbon nano-adsorbent. Fig. 7 shows that the adsorption efficiency of metal ions increases with increase in pH value from 2 to 6, and the highest removal efficiency was observed at pH 6 for nickel and cobalt ions. Because the number of hydrogen ions decreased in the solution and the competition between hydrogen ions and metal ions declined. At higher pH values, the concentration of H^+ decreased and the concentration of OH^- increased, the (OH^-) ions formed complexes with the metal ions in the solution, and these complexes precipitated and their solubility in the solution declined. Therefore, the hydroxide ions competed with the metal ions for occupying the active sites on the adsorbent surface. Therefore, this led to a reduction in the adsorption of metal ions on the adsorbent surface.

The highest adsorption efficiencies of nickel and cobalt ions using the AC/Fe_3O_4 nano-adsorbent at pH 6 were obtained 90.3% and 90.1%, respectively. Therefore, pH 6 was considered the optimum pH value.

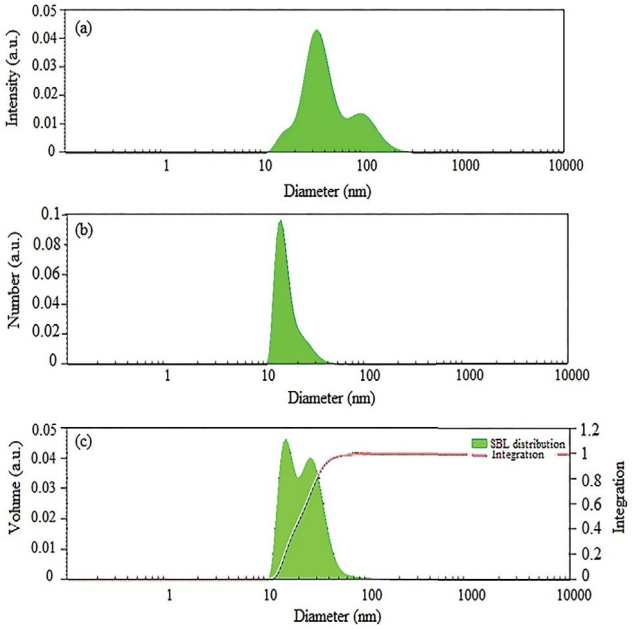

Fig. 6. Magnetic activated carbon nano-adsorbent analyzed using DLS and employing the SBL analytical method in terms of intensity (a), particles number (b), and volume (c).

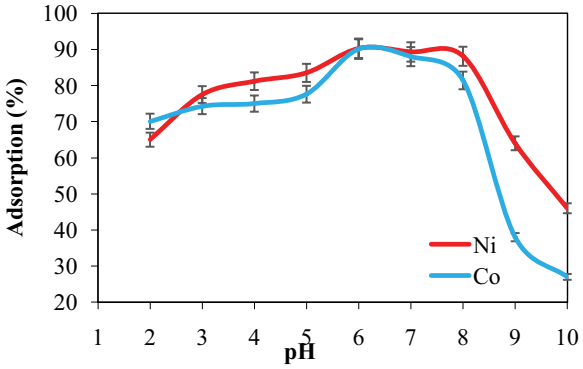

Fig. 7. Effect of pH on the removal of nickel and cobalt ions (other conditions: an initial ion concentration of 10 mg/L, temperature of 25°C, adsorbent dose of 0.3 g/L, contact time of 70 min, and mixing speed of 200 rpm).

3.3. Impact of buffer type and volume

Fig. 8 presents the effect of various buffers on the removal efficiency of nickel and cobalt ions. The results indicate that the adsorbed quantity in the presence of the maleic acid buffer well matches that observed at optimum pH value, whereas phosphate, citrate, and potassium hydrogen phthalate buffers interfere with this measurement method.

Also, Fig. 9 demonstrates the effect of buffer volume in removing nickel and cobalt ions from aqueous solution using the AC/Fe_3O_4 composite. As shown in Fig. 9, there is an ascending trend in nickel and cobalt ion removal when 0–1 mL of the maleic acid buffer was used, but no tangible changes happened in removal efficiency when larger volumes of the maleic acid buffer were utilized. Therefore,

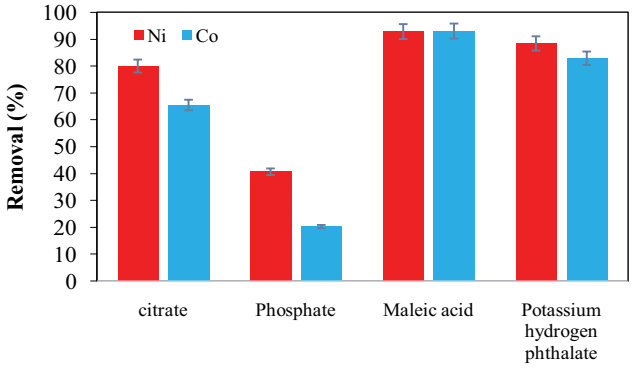

Fig. 8. Effect of various buffers on the removal of nickel and cobalt ions (other conditions: an initial ion concentration of 10 mg/L, pH of 6, adsorbent dose of 0.3 g/L, contact time of 70 min, and mixing speed of 200 rpm).

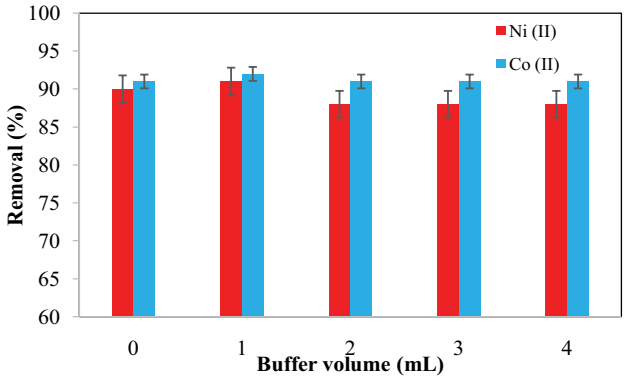

Fig. 9. Effect of maleic acid volume in removing nickel and cobalt ions (other conditions: an initial ion concentration of 10 mg/L, pH of 6, adsorbent dose of 0.3 g/L, contact time of 70 min, and mixing speed of 200 rpm).

1 mL of the maleic acid buffer solution was considered as the optimum buffer volume which in this condition, 92% and 91% of Co(II) and Ni(II) were removed.

3.4. Impact of temperature

Fig. 10 shows the impact of various temperatures (25°C, 35°C, 45°C, and 55°C) on the removal of nickel and cobalt ions from aqueous solution. The removal percentage of these ions declined when the temperature increased from 25°C to 55°C. This reduction was due to the increased movement of molecules. The adsorption rate increases with an increase in the movement of molecules. However, it is more difficult to separate the nickel and cobalt ions that have been adsorbed on the nano-adsorbent surface when a higher temperature is applied to the solution. This shows that the adsorption process of nickel and cobalt ions on the adsorbent surface is exothermic. Moreover, the lower the temperature, the more cost-effective the adsorption process.

The highest adsorption efficiencies of Ni(II) and Co(II) ions by the magnetic nano-adsorbent at 25°C were obtained 91% and 92%, respectively. Therefore, 25°C was considered the optimum adsorption temperature.

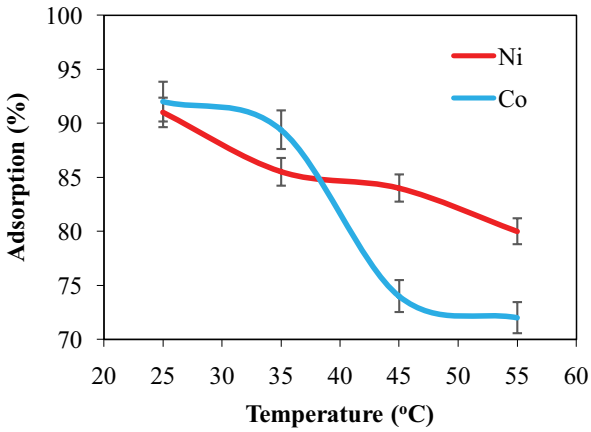

Fig. 10. Effects of temperature on removing nickel and cobalt ions (other conditions: an initial ion concentration of 10 mg/L, pH of 6, adsorbent dose of 0.3 g/L, contact time of 70 min, and mixing speed of 200 rpm).

3.5. Impact of adsorbent dose

The adsorbent dosage is a critical factor in the sorption process, because this factor determines the adsorption capacity of an adsorbent. The impact of adsorbent dose on the sorption efficiency of Ni(II) and Co(II) ions are demonstrated in Fig. 11. Other conditions were kept constant including temperature of 25°C, initial ion concentration of 10 mg/L, pH of 6, and contact time of 70 min. As shown in this figure, the sorption efficiency was increased by increasing composite dose from 0.1 to 0.5 g/L. In the adsorbent dose above 0.5 g/L, no significant changes were observed in the removal efficiency of Ni(II) and Co(II). Because by increasing the adsorbent dosage, the active sites on the surface of the nano-composite will increase, which results in further adsorption of metal ions on the surface of the adsorbent [24]. Therefore, the adsorbent dose of 0.5 g/L was considered as the optimal value, which in this adsorbent dose, the removal efficiency of Ni(II) and Co(II) was determined 93.5% and 94.8%, respectively.

3.6. Impact of contact time

Contact time is another important factor on the adsorption efficiency. The impact of contact time on the removal efficiency of Ni(II) and Co(II) from aqueous solution using the AC/Fe_3O_4 nano-composite is illustrated in Fig. 12. The experiments were done in a temperature of 25°C, metal ions concentration of 10 mg/L, sorbent dosage of 0.5 g/L, and pH of 6. As shown in Fig. 12, the adsorption efficiency was increased by enhancing the contact time from 10 to 70 min for both metal ions, and at contact time above 70 min, the adsorption efficiency was slightly increased.

3.7. Reusability of the adsorbent

The reusability of the nano-adsorbent is a crucial factor for its industrial applications. In this investigation, the reusability of the AC/Fe_3O_4 nanocomposite after adsorption of heavy metal (Ni(II) and Co(II)) ions were studied

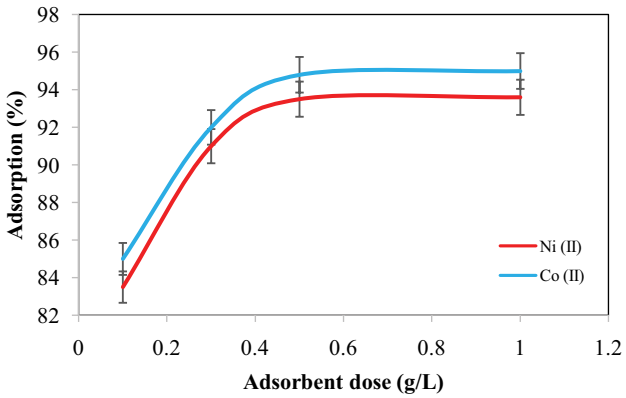

Fig. 11. Effect of adsorbent dose on the adsorption efficiency of Ni(II) and Co(II) using the AC/Fe_3O_4 nano-composite (other conditions: an initial ion concentration of 10 mg/L, pH of 6, temperature of 25°C, contact time of 70 min, and mixing speed of 200 rpm).

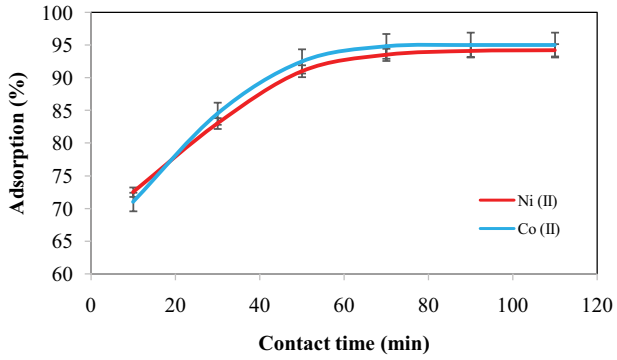

Fig. 12. Impact of contact time on the sorption of Ni(II) and Co(II) using the AC/Fe_3O_4 nano-composite (other conditions: an initial ion concentration of 10 mg/L, pH of 6, adsorbent dose of 0.5 g/L, temperature of 25°C, and mixing speed of 200 rpm).

in seven cycles. After the sorption process in each step, the nano-composite was separated from the aqueous media and washed several times with distilled water. Afterwards, the composite was washed by 20 mL of methanol/acetone with a molar ratio of 1:1 to remove Co(II) and Ni(II) ions from the surface of the nano-composite. After washing the adsorbent, it was reused in the sorption of Co(II) and Ni(II) ions. It is worth mentioning that the adsorption process in each cycle was done at optimized conditions. The results of adsorption/desorption process using the aforementioned nano-adsorbent are demonstrated in Fig. 13. The reduction in the sorption efficiency of Co(II) and Ni(II) ions using the AC/Fe_3O_4 nano-composite was less than 5% after five cycles of adsorption/desorption process. The results of adsorption efficiency showed that the AC/Fe_3O_4 nano-adsorbent can be used for five cycles of sorption/desorption process. Therefore, the results indicated that the aforementioned nano-adsorbent can be used as an appropriate adsorbent for the removal of Co(II) and Ni(II) ions from aqueous solution.

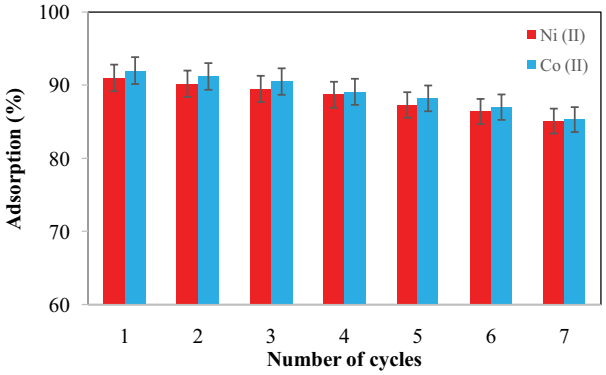

Fig. 13. Adsorption/desorption studies of Co(II) and Ni(II) ions using AC/Fe_3O_4 nanocomposite (conditions: an initial ion concentration of 10 mg/L, pH of 6, temperature of 25°C, adsorbent dose of 0.3 g/L, contact time of 70 min, and mixing speed of 200 rpm).

3.8. Adsorption isotherm

To explain the interaction between adsorbent and contaminants, adsorption isotherms are widely used and play a prominent role in the optimal use of adsorbents [17,23]. In this study, Langmuir and Freundlich isotherm models were applied to explain sorption of nickel and cobalt ions using the AC/Fe_3O_4 nano-adsorbent.

The Langmuir isotherm model states that adsorption of ions occurs on a single and homogeneous layer of adsorbent without any interaction between adjoining sites. This model provides the information about the adsorption capacity as well as the equilibrium behavior of the adsorption process [17,29]. The linear form of the Langmuir equation is as follows:

$$\frac{C_e}{q_e} = \frac{1}{K_L q_m} + \frac{C_e}{q_m} \tag{2}$$

where C_e, q_e, q_m, and K_L are equilibrium concentration of metal ion in solution (mg/L), equilibrium adsorption capacity (mg/g), the utmost adsorption capacity (mg/g), and adsorption energy or Langmuir constant (L/g), respectively. Moreover, a constant parameter namely separation factor (R_L) is defined as Eq. (3):

$$R_L = \frac{1}{1 + K_L C_i} \tag{3}$$

In this equation, C_i is the initial concentration of metals ion (mg/g). If $R_L > 1$, $R_L = 0$, $R_L = 1$, and $0 < R_L < 1$, the sorption process is categorized as undesirable, irreversible, linear, and desirable, respectively [17,23].

The Freundlich model is another isotherm model. This model is applied to describe multi-layer sorption on heterogeneous surfaces. The linear form of this model is expressed as follows:

$$\mathrm{Ln}q_e = \mathrm{Ln}K_F + \frac{1}{n}\mathrm{Ln}C_e \tag{4}$$

where K_F is a constant depending on sorption capacity and n is an empirical parameter related to adsorption intensity. In the Freundlich isotherm model, for $n > 1$ and $1 < n < 10$, the adsorption process is undesirable and desirable, respectively [17]. The results of the Langmuir and Freundlich isotherm models are shown in Table 3. Also, Fig. 14 is plotted for the Langmuir and Freundlich models.

The results of the mentioned isotherms indicated that the Freundlich isotherm has a higher correlation coefficient (R^2). Therefore, the adsorption process of cobalt and nickel ions on the adsorbent surface followed the Freundlich model, and hence, the adsorption took place on a multi-layer surface.

According to Table 3, the highest adsorption capacities for the nickel and cobalt ions using the Langmuir model were obtained 212.76 and 204.08 mg/g, respectively. Moreover, the R_L value obtained from the Langmuir model showed that the adsorption process of the two metal ions was performed favorably. Furthermore, the value of "n" in the Freundlich model for the two metal ions indicated that the adsorption process took place physically.

The maximum sorption capacity of Ni(II) and Co(II) using the AC/Fe_3O_4 nanocomposite was compared to previous studies and the results are presented in Table 4. As reported in this Table 4, the maximum adsorption capacity in this study for the adsorption of both heavy metals were higher than previous studies, which shows that the nanocomposite used in this work has a high ability to remove heavy metals from aqueous solution and can be utilized as a strong adsorbent in the future works.

3.9. Kinetic study

To study the kinetic behavior of the Ni(II) and Co(II) ions uptake process from the aqueous media using the AC/Fe_3O_4 nano-composite, pseudo-first-order, pseudo-second-order, intraparticle diffusion kinetic models were used and the linear form of these models are presented as follows [33,34]:

$$\ln\left(q_{eq} - q_t\right) = \ln q_{eq.cal} - K_1 t \tag{5}$$

$$\frac{t}{q_t} = \frac{1}{K_2 q_{eq}^2} + \frac{t}{q_{e.cal}} \tag{6}$$

$$q_t = K_I t^{0.5} + I \tag{7}$$

where q_{eq} (mg/g) and q_t (mg/g) are the adsorbed value of metal ions per gram of the adsorbent at equilibrium time and time t, respectively. Also, K_1 and K_2 are the sorption kinetic constants for the PFO (1/min) and PSO kinetic models (g/mg min), respectively. Moreover, K_I and I are the intraparticle diffusion rate constant (mg/g $min^{0.5}$) and the boundary layer thickness, respectively. The results of the kinetic study are demonstrated in Fig. 15 and the constants and parameters of these models are presented in Table 5. The effect of contact time was used to study the kinetic behavior of the sorption process. According to the results of the kinetic study, the PSO kinetic model with correlation coefficients of 0.9992 and 0.9987 for Ni(II) and Co(II) could better described the kinetic behavior of the sorption process compared to PFO and intraparticle diffusion kinetic models. Also, to find whether the intraparticle diffusion kinetic model is the main stage in controlling

Table 3
Results obtained from Langmuir and Freundlich isotherms for removal of nickel and cobalt ions from aqueous solution using the nano-composite

Model	Parameter	Co(II)	Ni(II)
Langmuir	R^2	0.9945	0.8982
	R_L	0.739	0.734
		0.586	0.579
		0.415	0.408
		0.262	0.256
	q_{max} (mg/g)	204.08	212.76
	K_L	0.0704	0.0726
Freundlich	R^2	0.9983	0.9993
	K_F	13.65	14.89
	n	1.18	1.21

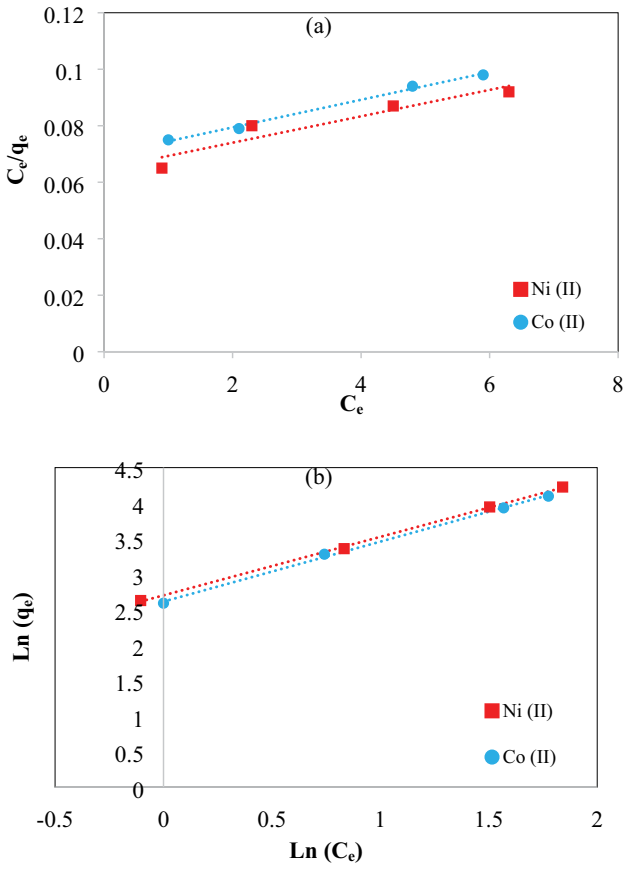

Fig. 14. Langmuir (a) and Freundlich (b) isotherm models for the removal of Ni(II) ion and Co(II) ion from aqueous solution using the AC/Fe_3O_4 nano-adsorbent (conditions: pH of 6, temperature of 25°C, adsorbent dose of 0.3 g/L, contact time of 70 min, and mixing speed of 200 rpm).

Table 4
Comparing the results with previous studies

Adsorbent	q_{max} for Ni(II)	q_{max} for Co(II)	Reference
Sheep manure wastes	7.2	–	[3]
Seaweeds	18.58	20.63	[6]
Kaolinite	1.669	0.919	[9]
Activated carbon prepared by worn tires	109.89	90.09	[12]
Bentonite/Fe_3O_4 nanocomposite	5.98	–	[16]
Hydroxyapatite	18.6	22.5	[30]
Pre-treated 2-Hypnea Valentiae algae biomass	–	16.66	[31]
Raw algae biomass	–	10.98	[31]
Calcium alginate/spent coffee grounds composite	20.96	–	[32]
AC/Fe_3O_4	212.76	204.08	Present study

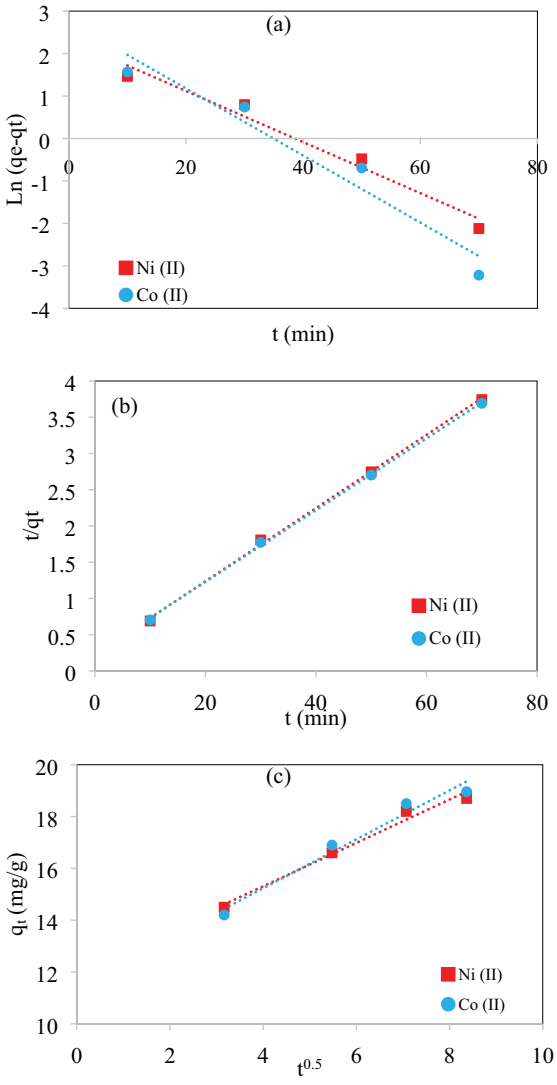

Fig. 15. Kinetic behavior of the sorption process including (a) PFO, (b) PSO, and (c) intraparticle diffusion kinetic models (conditions: an initial ion concentration of 10 mg/L, pH of 6, adsorbent dose of 0.5 g/L, temperature of 25°C, and mixing speed of 200 rpm).

the adsorption process of Ni(II) and Co(II) onto AC/Fe_3O_4 nano-adsorbent, the experimental data were fitted with the kinetic model of intraparticle diffusion. According to the results, this model showed that Ni(II) and Co(II) was probably transported from the aqueous solution to the composite surface by intraparticle diffusion. Since the intercept of the intraparticle diffusion model is not zero, the intraparticle diffusion may be part of the uptake process but it's not just the controlling rate of the sorption process. Other mechanisms such as complexes or ion-exchange influence controlling rate of the Ni(II) and Co(II) adsorption [33].

3.10. Thermodynamic studies

To calculate the changes of Gibbs free energy ($\Delta G°$), entropy ($\Delta S°$), and enthalpy ($\Delta H°$), Eqs. (8) and (9) were used [17,23]:

$$\Delta G° = -RT \ln K_d \tag{8}$$

$$\ln K_d = \left(\frac{\Delta S°}{R}\right) - \left(\frac{\Delta H°}{RT}\right) \tag{9}$$

where R, T (K), and K_d (q_e/c_e) are the gas universal constant, temperature and distribution coefficient, respectively. To study the thermodynamic behavior of the sorption process, the experiments were done in different temperatures (25°C, 35°C, 45°C, and 55°C). Other factors were kept constant including initial ion concentrations of 10 mg/L, pH of 6, contact time of 70 min, and mixing speed of 200 rpm.

Fig. 16 shows the plot of $\ln K_d$ against $1/T$. The values of $\Delta H°$ and $\Delta S°$ are calculated from the slope and intercept of Fig. 16. Constants and parameters of the thermodynamic study are presented in Table 6.

The results showed that the values of $\Delta G°$ at different temperatures were obtained negative for the nickel and cobalt ions, which showed that the adsorption process of the two ions by the magnetic activated carbon nano-adsorbent was spontaneous. Moreover, $\Delta G°$ decreased with increasing temperature. This suggested that the aforementioned adsorbent was also able to adsorb these two metal ions at higher temperatures. Furthermore, the value of $\Delta H°$ for the

Table 5
Constants and parameters of the kinetic models of the sorption process

	PFO		PSO		Intraparticle diffusion	
Ni(II)	$q_{e,cal}$ (mg/g)	15.786	$q_{e,cal}$ (mg/g)	20.2	K_I (mg/g min$^{0.5}$)	0.9443
	K_1 (1/min)	0.079	K_2 (g/mg min)	0.0102	I (mg/g)	11.456
	R^2	0.9445	R^2	0.9992	R^2	0.9694
Co(II)	$q_{e,cal}$ (mg/g)	10.184	$q_{e,cal}$ (mg/g)	19.8	K_I (mg/g min$^{0.5}$)	0.8368
	K_1 (1/min)	0.06	K_2 (g/mg min)	0.0112	I (mg/g)	11.963
	R^2	0.9677	R^2	0.9987	R^2	0.9826

Table 6
Thermodynamic parameters for adsorption of nickel and cobalt ions using the adsorbent

Parameter	Cobalt	Nickel$^+$	Temperature (K)
$\Delta G°$ (KJ/mol)	–6.1926	–5.5253	298.15
	–4.8737	–4.9161	308.15
	–3.5548	–4.3068	318.15
	–2.2358	–3.6976	328.15
$\Delta H°$ (KJ/mol)	–45.5166	–23.6899	298.15–328.15
$\Delta G°$ (J/mol K)	–131.8932	–60.9241	298.15–328.15

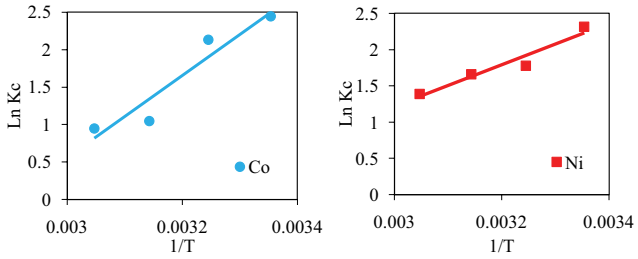

Fig. 16. Thermodynamic model for the removal of cobalt and nickel ions from aqueous solutions by using the magnetic nano-adsorbent (other conditions: an initial ion concentration of 10 mg/L, pH of 6, adsorbent dose of 0.3 g/L, contact time of 70 min, and mixing speed of 200 rpm).

sorption of Ni(II) and Co(II) ions was obtained negative, which indicates that the sorption process is exothermic.

4. Conclusion

In this research, the adsorption process of cobalt and nickel ions from aqueous solutions was studied using the activated carbon/Fe_3O_4 nano-adsorbent. Several analyses such as SEM, FTIR, BET, DLS, and XRD were performed to determine the surface properties of the nano-adsorbent. Also, the effect of various parameters such as pH 2–10, temperature (25°C–55°C), contact time (10–110 min), adsorbent dosage (0.1–1 g/L), and buffer type was studied on the removal of Co(II) and Ni(II) ions from aqueous solution. Moreover, the equilibrium, kinetic, and thermodynamic studies of the adsorption process were done to investigate the adsorption process behavior. To study the equilibrium behavior of the adsorption process, Langmuir, and Freundlich isotherm models were investigated. Of these two isotherm models, the Freundlich isotherm was more desirable for the two metal ions because of its higher correlation coefficient (R^2) compared to that of the Langmuir model. It was observed that the adsorption process of the two metal ions by the nano-adsorbent was physical. Furthermore, the thermodynamic study showed that the adsorption process of these two metal ions was spontaneous and irreversible. Besides, the negative value of enthalpy indicated that the adsorption process was exothermic.

References

[1] F. Fu, Q. Wang, Removal of heavy metal ions from wastewaters: a review, J. Environ. Manage., 92 (2011) 407–418.
[2] A.H. Mahvi, Application of agricultural fibers in pollution removal from aqueous solution, Int. J. Environ. Sci. Technol., 5 (2008) 275–285.
[3] H.J. Mansoorian, A. Rajabizadeh, E. Bazrafshan, A.H. Mahvi, Practical assessment of electrocoagulation process in removing nickel metal from aqueous solutions using iron-rod electrodes, Desal. Water Treat., 44 (2012) 29–35.
[4] F. Abu Al-Rub, M. Kandah, N. Al-Dabaybeh, Competitive adsorption of nickel and cadmium on sheep manure wastes: experimental and prediction studies, Sep. Sci. Technol., 38 (2003) 483–497.
[5] C.E. Borba, R. Guirardello, E.A. Silva, M.T. Veit, C.R.G. Tavares, Removal of nickel(II) ions from aqueous solution by biosorption in a fixed bed column: experimental and theoretical breakthrough curves, Biochem. Eng. J., 30 (2006) 184–191.
[6] K. Vijayaraghavan, J. Jegan, K. Palanivelu, M. Velan, Biosorption of cobalt(II) and nickel(II) by seaweeds: batch and column studies, Sep. Purif. Technol., 44 (2005) 53–59.
[7] S.I. El-Dessouky, E.A. El-Sofany, J.A. Daoud, Studies on the sorption of praseodymium(III), holmium(III) and cobalt(II) from nitrate medium using TVEX–PHOR resin, J. Hazard. Mater., 143 (2007) 17–23.
[8] D. Xu, D. Shao, C. Chen, A. Ren, X. Wang, Effect of pH and fulvic acid on sorption and complexation of cobalt onto bare and FA bound MX-80 bentonite, Radiochim. Acta, 94 (2006) 97–102.
[9] O. Yavuz, Y. Altunkaynak, F. Guzel, Removal of copper, nickel, cobalt and manganese from aqueous solution by kaolinite, Water Res., 37 (2003) 948–995.
[10] S. Rengaraj, S. Moon, Kinetics of adsorption of Co(II) removal from water and wastewater by ion exchange resins, Water Res., 36 (2002) 1783–1793.
[11] R. Rezaei Kalantry, A. Jonidi Jafari, A. Esrafili, B. Kakavandi, A. Gholizadeh, A. Azari, Optimization and evaluation of reactive dye adsorption on magnetic composite of activated carbon and iron oxide, Desal. Water Treat., 57 (2016) 6411–6422.
[12] S. Abbasi, R. Foroutan, H. Esmaeili, F. Esmaeilzadeh, Preparation of activated carbon from worn tires for removal of Cu(II), Ni(II) and Co(II) ions from synthetic wastewater, Desal. Water Treat., 141 (2019) 269–278.

[13] A.H. Mahvi, F. Gholami, S. Nazmara, Cadmium biosorption from wastewater by Ulmus leaves and their ash, Eur. J. Sci. Res., 23 (2008) 197–203.
[14] M.M. Boushehrian, H. Esmaeili, R. Foroutan, Ultrasonic assisted synthesis of Kaolin/$CuFe_2O_4$ nanocomposite for removing cationic dyes from aqueous media, J. Environ. Chem. Eng., 8 (2020) 103869, doi: 10.1016/j.jece.2020.103869.
[15] M. Ahmadi, M.H. Niari, B. Kakavandi, Development of maghemite nanoparticles supported on cross-linked chitosan (γ-Fe_2O_3@CS) as a recoverable mesoporous magnetic composite for effective heavy metals removal, J. Mol. Liq., 248 (2017) 184–196.
[16] F. Ahmadi, H. Esmaeili, Chemically modified bentonite/Fe_3O_4 nanocomposite for Pb(II), Cd(II), and Ni(II) removal from synthetic wastewater, Desal. Water Treat., 110 (2018) 154–167.
[17] S. Tamjidi, H. Esmaeili, B.K. Moghadas, Application of magnetic adsorbents for removal of heavy metals from wastewater: a review study, Mater. Res. Express, 6 (2019) 102004, doi: 10.1088/2053-1591/ab3ffb.
[18] S. Tamjidi, H. Esmaeili, Chemically modified CaO/Fe_3O_4 nanocomposite by Sodium dodecyl sulfate for Cr(III) removal from water, Chem. Eng. Technol., 42 (2019) 607–616.
[19] R. Rezaei Kalantary, E. Dehghanifard, A. Mohseni-Bandpi, L. Rezaei, A. Esrafili, B. Kakavandi, A. Azari, Nitrate adsorption by synthetic activated carbon magnetic nanoparticles: kinetics, isotherms and thermodynamic studies, Desal. Water Treat., 57 (2016) 16445–16455.
[20] A. Ahmadi, R. Foroutan, H. Esmaeili, S. Tamjidi, The role of bentonite clay and bentonite clay@$MnFe_2O_4$ composite and their physico-chemical properties on the removal of Cr(III) and Cr(VI) from aqueous media, Environ. Sci. Pollut. Res., 27 (2020) 14044–14057.
[21] M.T. Bankole, A.S. Abdulkareem, I.A. Mohammed, S.S. Ochigbo, J.O. Tijani, O.K. Abubakre, W.D. Roos, Selected heavy metals removal from electroplating wastewater by purified and polyhydroxylbutyrate functionalized carbon nanotubes adsorbents, Sci. Rep., 9 (2019) 1–19.
[22] A. Azari, H. Gharibi, B. Kakavandi, G. Ghanizadeh, A. Javid, A.H. Mahvi, K. Sharafi, T. Khosravia, Magnetic adsorption separation process: an alternative method of mercury extracting from aqueous solution using modified chitosan coated Fe_3O_4 nanocomposites, J. Chem. Technol. Biotechnol., 92 (2017) 188–200.
[23] R. Foroutan, R. Mohammadi, S. Farjadfard, H. Esmaeili, B. Ramavandi, G.A. Sorial, Eggshell nano-particle potential for methyl violet and mercury ion removal: surface study and field application, Adv. Powder Technol., 30 (2019) 2188–2199.
[24] R. Foroutan, A. Oujifard, F. Papari, H. Esmaeili, Calcined *Umbonium vestiarium* snail shell as an efficient adsorbent for treatment of wastewater containing Co(II), 3Biotech, 9 (2019), doi: 10.1007/s13205-019-1575-1.
[25] W. Tian, H. Li, J. Zhou, Y. Guo, Preparation, characterization and the adsorption characteristics of lignin/silica nanocomposites from cellulosic ethanol residue, RSC Adv., 7 (2017) 41176–41181.
[26] O. Plohl, M. Finšgar, S. Gyergyek, U. Ajdnik, I. Ban, L.F. Zemljič, Efficient copper removal from an aqueous anvironment using a novel and hybrid nanoadsorbent based on derived-polyethyleneimine linked to silica magnetic nanocomposites, Nanomaterials, 9 (2019), doi: 10.3390/nano9020209.
[27] M.J. Livani, M. Ghorbani, Fabrication of $NiFe_2O_4$ magnetic nanoparticles loaded on activated carbon as novel nano-adsorbent for Direct Red 31 and Direct Blue 78 adsorption, Environ. Technol., 39 (2018) 2977–2993.
[28] S. Yadav, D. Singh, S. Sinha, Chemical carbonization of papaya seed originated charcoals for sorption of Pb(II) from aqueous solution, J. Environ. Chem. Eng., 2 (2014) 9–19.
[29] H. Esmaeili, R. Foroutan, Adsorptive behavior of methylene blue onto sawdust of sour lemon, date palm, and eucalyptus as agricultural wastes, J. Dispersion Sci. Technol., 40 (2019) 990–999.
[30] M. Ferri, S. Campisi, A. Gervasini, Nickel and cobalt adsorption on hydroxyapatite: a study for the de-metalation of electronic industrial wastewaters, Adsorption, 25 (2019) 649–660.
[31] L. Vafajoo, R. Cheraghi, R. Dabbagh, G. McKay, Removal of cobalt(II) ions from aqueous solutions utilizing the pre-treated 2-Hypnea Valentiae algae: equilibrium, thermodynamic, and dynamic studies, Chem. Eng. J., 331 (2018) 39–47.
[32] R. Torres-Caban, C.A. Vega-Olivencia, N. Mina-Camilde, Adsorption of Ni^{2+} and Cd^{2+} from water by calcium alginate/spent coffee grounds composite beads, Appl. Sci., 9 (2019) 4531, doi: 10.3390/app9214531.
[33] E.K. Pasandideh, B. Kakavandi, S. Nasseri, A.H. Mahvi, R. Nabizadeh, A. Esrafili, R.R. Kalantary, Silica-coated magnetite nanoparticles core-shell spheres (Fe_3O_4@SiO_2) for natural organic matter removal, J. Environ. Health Sci., 14 (2016) 21.
[34] B. Kakavandi, A. Jonidi Jafari, R. Rezaei Kalantary, S. Nasseri, A. Esrafili, A. Gholizadeh, A. Azari, Simultaneous adsorption of lead and aniline onto magnetically recoverable carbon: optimization, modeling and mechanism, J. Chem. Technol. Biotechnol., 91 (2016) 3000–3010.